

November 6, 2018  
 BI-TP 2001/14

## Spectrum of the Dirac Operator coupled to two-dimensional quantum gravity

L. Bogacz<sup>1,2</sup>, Z. Burda<sup>1,2</sup>, C. Petersen<sup>1</sup> and B. Petersson<sup>1</sup>

<sup>1</sup>Fakultät für Physik, Universität Bielefeld  
 P.O.Box 100131, D-33501 Bielefeld, Germany

<sup>2</sup>Institute of Physics, Jagellonian University  
 ul. Reymonta 4, 30-059 Krakow, Poland

### Abstract

We implement fermions on dynamical random triangulation and determine numerically the spectrum of the Dirac-Wilson operator  $\mathcal{D}$  for the system of Majorana fermions coupled to two-dimensional Euclidean quantum gravity. We study the dependence of the spectrum of the operator  $\epsilon\mathcal{D}$  on the hopping parameter. We find that the distributions of the lowest eigenvalues become discrete when the hopping parameter approaches the value  $1/\sqrt{3}$ . We show that this phenomenon is related to the behavior of the system in the 'antiferromagnetic' phase of the corresponding Ising model. Using finite size analysis we determine critical exponents controlling the scaling of the lowest eigenvalue of the spectrum including the Hausdorff dimension  $d_H$  and the exponent  $\kappa$  which tells us how fast the pseudo-critical value of the hopping parameter approaches its infinite volume limit.

## Introduction

The dynamical triangulation approach to quantum gravity has proven to be a very powerful method [1, 2, 3]. In two-dimensions it yields the same results for critical exponents as the Liouville theory [4, 5, 6]. Contrary to the latter, this approach can be straightforwardly generalized to higher dimensional case which is frequently referred to as simplicial gravity [7, 8]. Results from numerical studies of pure gravity without matter fields in four dimensions showed that the continuum limit of this model does not exist [9]. In order

to obtain more realistic models, one has tried to include matter fields and to couple them to gravity [10]. This program has so far succeeded only for bosonic matter. Putting fermions on random simplicial manifold is a more difficult task. In general it requires introducing an additional field of local frames in order to define a spin structure [11, 12, 13]. In the case of a compact manifold this is a topological problem. Although many ingredients of the construction are known and can be generalized to any number of dimensions, the topological part of the problem has been solved so far only in two dimensions [13, 14].

In this paper we will study properties of the Dirac-Wilson operator on two-dimensional dynamical triangulation with spherical topology. The analysis of the spectrum in the critical region allows us to calculate critical indices as for example the Hausdorff dimension.

We cross-check properties of the spectrum using the fact that the partition function of the fermionic model can be mapped into the partition function of Ising model on dynamical triangulation, which is analytically solvable [15, 16, 17].

The spectrum of the Majorana-Dirac-Wilson operator  $\epsilon\mathcal{D}$  becomes discrete when the hopping parameter admits the value  $1/\sqrt{3}$  corresponding to the value  $\beta = 0$  of the coupling in the Ising model. We show that this behaviour can be explained by the presence of a set of points in 'antiferromagnetic' phase ( $\beta < 0$ ), for which some eigenvalues of the operator are determined by local properties of the triangulation and not by its random character.

The paper is organized as follows : First we define the model, then we recall some facts about its relation to the Ising model [12], we present results of numerical studies and shortly conclude at the end by summarizing and listing open questions. In the appendix, for comparison, we calculate the spectrum of the Dirac-Wilson operator on a regular triangulation.

## The model

The model of fermions minimally coupled to Euclidean gravity is given by the partition function

$$\mathcal{Z} = \sum_{T \in \mathcal{T}} \mathcal{Z}_T = \sum_{T \in \mathcal{T}} \int \prod_i d\bar{\Psi}_i d\Psi_i e^{-S_T} \quad (1)$$

where the sum goes over  $d$ -dimensional simplicial manifolds from a class  $\mathcal{T}$ , say, for instance, with spherical topology. Each triangulation is dressed with the fermion field located in the centers of  $d$ -simplices. The integral over field

on a given triangulation  $T$  defines the partition function  $\mathcal{Z}_T$ , which at the same time provides a weight of this triangulation in the ensemble. The action reads

$$S_T = -K \sum_{\langle ij \rangle} \bar{\Psi}_i \mathcal{H}_{ij} \Psi_j + \frac{1}{2} \sum_i \bar{\Psi}_i \Psi_i = \sum_{i,j} \bar{\Psi}_i \mathcal{D}_{ij} \Psi_j, \quad (2)$$

where the fermionic fields  $\Psi_i$  are located in the centers of triangles. The sum over  $\langle ij \rangle$  runs over oriented pairs of neighboring triangles, or equivalently, over oriented dual links. The hopping operator is

$$\mathcal{H}_{ij} = \frac{1}{2} (1 + n_{ij}^{(i)} \cdot \gamma) \mathcal{U}_{ij}. \quad (3)$$

The Dirac-Wilson operator is denoted by  $\mathcal{D}_{ij}$  and the spin connection by  $\mathcal{U}_{ij}$ . In order to be able to calculate spinor and vector components, we endow each  $d$ -simplex with an orthonormal local frame. A frame is a set of orthonormal oriented vectors  $e_a$ ,  $a = 1, \dots, d$ . To each vector  $e_a$  we ascribe a Dirac gamma matrix  $\gamma^a$ , in such a way that its numerical value is identical in each frame. The local vector  $n_{ij}$  in eq. (3) is a unit vector which points from the center of the simplex  $j$  to the center of one of its neighbors  $i$ . It just tells us the direction of the local derivative. The inner product of this vector and of gamma matrices, which is denoted by dot in (3), has to be understood as a sum of gamma matrices  $\gamma^a$  multiplied by the components of  $[n_{ij}^{(i)}]_a$  in the given frame at  $i$ , denoted by the upper index. Thus, the product of the same vector  $n_{ij}$  expressed in another frame yields a different matrix:  $n_{ij}^{(j)} \cdot \gamma = [n_{ij}^{(j)}]_a \gamma^a$ .

As mentioned the matrix  $\mathcal{U}_{ij}$  plays the role of spin connection. It allows us to parallel transport a spinor from the simplex  $j$  to the simplex  $i$ , or in other words, to recalculate spinor components between two neighboring frames  $i$  and  $j$ . The matrix  $\mathcal{U}_{ij}$  is an image in the spinorial representation of the rotation matrix  $U_{ij}$  which parallel transports vectors. The map  $U_{ij} \rightarrow \mathcal{U}_{ij}$  is not unique, namely it is defined up to sign. As we will see below, the signs of  $\mathcal{U}$  must be adjusted to fulfill a consistency condition (8) for all elementary plaquettes of the simplicial manifold. This is a topological problem.

This problem has been solved in two-dimensions where an explicit construction of the signs of the spin connection matrices  $\mathcal{U}_{ij}$  has been given [13]. Let us shortly recall the main steps of the construction.

In two dimensions each orthonormal frame consists of two vectors  $e_{ia}$  where  $a$  is 1 or 2. The first index of  $e_{ia}$  refers to the triangle in which the frame is located. For any pair of neighboring triangles  $i, j$  we can define a spin connection as a two by two rotation matrix  $[U_{ij}]_b^a$ , such that<sup>1</sup>  $e_{ia} =$

<sup>1</sup>In general a connection can be a dynamical field.

$\sum_b [U_{ij}]_a^b e_{jb}$ . Using matrix notation this relation can be written as  $e_i = U_{ij} e_j$ , where

$$U_{ij} = e^{\epsilon \Delta \phi_{ij}} = \begin{pmatrix} \cos \Delta \phi_{ij} & \sin \Delta \phi_{ij} \\ -\sin \Delta \phi_{ij} & \cos \Delta \phi_{ij} \end{pmatrix} \quad (4)$$

and  $\Delta \phi_{ij}$  is the relative angle between the two neighboring frames.  $\epsilon$  is the standard antisymmetric tensor.

The trace of an elementary loop around a dual plaquette is a geometrical invariant directly related to the curvature (deficit angle) of the vertex in the center of the plaquette. One can check that

$$\frac{1}{2} \text{Tr} UU \dots U = \frac{1}{2} \text{Tr} e^{\epsilon(2\pi - \Delta_P)} = \cos \Delta_P, \quad (5)$$

where  $\Delta_P$  is the deficit angle of the vertex in middle of the plaquette. The product  $UU \dots U$  of connections on all links on the plaquette perimeter  $P$  is a rotation matrix which gives the integrated rotation of a tangent vector parallel transported around this loop. The equation (5) is a sort of Wilson discretization [18, 19] of curvature calculated from the Cartan structure equations [20].

Now the idea is to write down an analogous equation as (5) in the spinorial representation. First we have to introduce a parallel transporter  $\mathcal{U}_{ij}$  for spinors for each pair of neighboring vertices. This is exactly the object which we need in (3). The connection  $\mathcal{U}_{ij}$  is an spinorial image of  $U_{ij}$ . One can choose a representation of gamma matrices such that  $U_{ij} = \mathcal{U}_{ij}^2$ . One immediately sees that indeed  $\mathcal{U}_{ij}$  can be calculated for a given  $U_{ij}$  up to sign. When defining the Dirac-Wilson operator (3) we cannot allow for ambiguities, so we have to give a unique prescription how to calculate  $\mathcal{U}_{ij}$ . We do this by choosing

$$\mathcal{U}_{ij} = e^{\frac{\epsilon \Delta \phi_{ij}}{2}} = \begin{pmatrix} \cos \frac{\Delta \phi_{ij}}{2} & \sin \frac{\Delta \phi_{ij}}{2} \\ -\sin \frac{\Delta \phi_{ij}}{2} & \cos \frac{\Delta \phi_{ij}}{2} \end{pmatrix} \quad (6)$$

and specifying the angles  $\Delta \phi_{ij}$  uniquely. More precisely we define  $\Delta \phi_{ij} = \phi_i^{(j)} - \phi_j^{(i)} + \pi$  where the angle  $\phi_i^{(j)}$  at triangle  $j$  is the angle between the vector  $e_{j1}$  of the frame at  $j$  and the vector  $n_{ij}$  (pointing from  $j$  to  $i$ ), and likewise  $\phi_j^{(i)}$  at triangle  $i$  is the angle between the vector  $e_{i1}$  and the vector  $n_{ji}$  (pointing from  $i$  to  $j$ ) (see fig.1). Both the angles are restricted to the range  $[0, 2\pi)$  and both are measured in the same direction, say clockwise. Thus the angle  $\Delta \phi_{ij}$  is defined without the  $2\pi$  ambiguity and hence the rotation matrix  $\mathcal{U}_{ij}$  is also uniquely determined including the total sign.

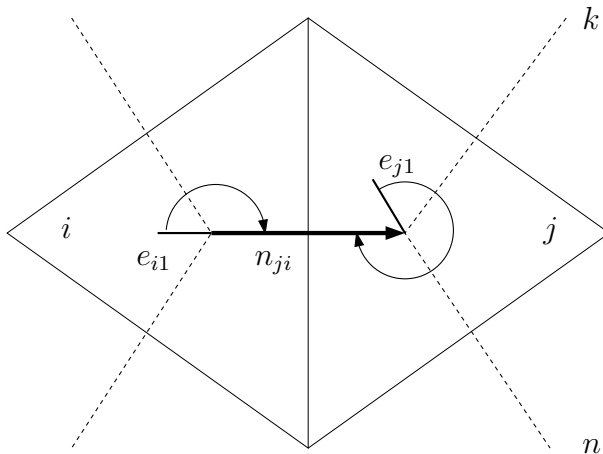


Figure 1: Local geometry of two neighboring triangles is shown. The position of the first frame vector  $e_1$  for a given triangle is marked by a line emerging from the triangle center. The position of the second frame vector  $e_2$  is implicitly given by the fact that the angle between  $e_1$  and  $e_2$  counted clockwise is  $\pi/2$ . The vector  $n_{ji}$  points from the center of the triangle  $i$  to  $j$ . The arch in the triangle  $i$  represents the angle  $\phi_j^{(i)}$  between  $e_{i1}$  and  $n_{ji}$ . The arch in the triangle  $j$  corresponds to the angle  $\phi_i^{(j)}$  between  $e_{j1}$  and  $n_{ij}$ . In the example shown in figure  $\phi_j^{(i)} = \pi$ ,  $\phi_i^{(j)} = 5\pi/3$ , and for other two neighbors of  $j$ :  $\phi_k^{(j)} = \pi/3$ ,  $\phi_n^{(j)} = \pi$ .

One can easily check that, for the definition (6) of  $\mathcal{U}_{ij}$ 's, the parallel transporter around an elementary loop gives

$$\frac{1}{2} \text{Tr} \mathcal{U} \mathcal{U} \dots \mathcal{U} = S_P \cos \frac{\Delta_P}{2}. \quad (7)$$

The argument of cosine got halved  $\Delta_P \rightarrow \Delta_P/2$  in comparison with (5) because for each link on  $P$  we have  $\mathcal{U}^2 = U$ . The total sign  $S_P$  of the product  $\mathcal{U} \mathcal{U} \dots \mathcal{U}$  has to be calculated. It turns out to depend on all angles  $\Delta\phi_{ij}$  on the loop and it may admit either value  $\pm 1$  [13].

The presence of elementary plaquettes which would have negative sign is an unwanted effect. For example, a spinor transported around a flat plaquette with  $S_P = -1$  would change the sign  $\psi \rightarrow -\psi$ . We require that the parallel transport around a close loop in a flat patch not change a spinor. Furthermore, we require the signs  $S_P$  to be positive for all elementary plaquettes

$$S_P = +1, \quad \forall P. \quad (8)$$

One can give the following argument in favor of the naturalness of this requirement. An elementary loop goes through triangles sharing a vertex. The geometry of a patch consisting of those triangles corresponds to the geometry of a cone. It is everywhere flat except at the vertex where it is singular. One can regularize such geometry by smoothing the peak of the cone (making it differentiable) in a very small region with radius  $\epsilon \approx 0$ . Such a regularization does not affect the loop which lies in a distance  $R \gg \epsilon$  from the vertex. Continuously shrinking the loop in such a regularized geometry, one can continuously change the angle of the loop rotation matrix without changing the sign. A completely shrunken loop must have positive sign since it lies in a flat patch. This implies  $S_P = +1$ . One can also check that the consistency condition (8) plays an essential role in the topological considerations or in deriving the equivalence with the Ising model.

The construction of the connections given in (6) does not fulfill the consistency condition (8). We will therefore modify the construction of  $\mathcal{U}$ 's by introducing for each link an additional sign degree of freedom  $s_{ij}$

$$\mathcal{U}_{ij} = s_{ij} e^{\frac{\epsilon \Delta \phi_{ij}}{2}}. \quad (9)$$

One can show that this freedom is sufficient to globally, for each elementary loop, fulfill the consistency condition (8), on a triangulation of an orientable manifold. Thus, technically, to define the Dirac-Wilson operator on a triangulation, we have to first assign an orthonormal frame to each triangle, and then for the frame assignment, to find link signs  $s_{ij}$  meeting the consistency condition (8) for each plaquette. The remaining part is straightforward. Namely, we express the operator  $\mathcal{U}_{ij}$  in terms of the angles  $\phi_i^{(j)}$  and  $\phi_j^{(i)}$  and likewise, the product  $n_{ij}^{(i)} \cdot \gamma$  in terms of  $\phi_j^{(i)}$ . Thus, we parameterize the hopping operator  $\mathcal{H}_{ij}$  entirely by  $\phi_i^{(j)}$  and  $\phi_j^{(i)}$  and  $s_{ij}$ . For each pair of neighboring triangles the angles can be read off from the given frame assignment (see fig.1).

Choosing the following representation of gamma matrices :  $\gamma_1 = \sigma_3$ ,  $\gamma_2 = \sigma_1$ , where the  $\sigma$  are Pauli matrices, we eventually arrive at

$$\mathcal{H}_{ij} = s_{ij} \cdot \begin{pmatrix} \sin \frac{\phi_j^{(i)}}{2} \cos \frac{\phi_i^{(j)}}{2} & \sin \frac{\phi_j^{(i)}}{2} \sin \frac{\phi_i^{(j)}}{2} \\ -\cos \frac{\phi_j^{(i)}}{2} \cos \frac{\phi_i^{(j)}}{2} & -\cos \frac{\phi_j^{(i)}}{2} \sin \frac{\phi_i^{(j)}}{2} \end{pmatrix}. \quad (10)$$

We see that in two dimensions the Dirac-Wilson operator on a triangulation  $T$  is given by a matrix consisting of two-by-two blocks

$$[\mathcal{D}_{ij}]_{\alpha}^{\beta} = \frac{1}{2} \delta_{ij} \delta_{\alpha}^{\beta} - K P_{ij} [\mathcal{H}_{ij}]_{\alpha}^{\beta} \quad (11)$$

where  $P_{ij}$  is an adjacency matrix :

$$P_{ij} = \begin{cases} 1, & \text{if } i, j \text{ are neighbors} \\ 0, & \text{otherwise} \end{cases} \quad (12)$$

There is no summation over  $ij$  in the equation (11). The blocks  $\mathcal{H}_{ij}$  have a very simple structure. In fact, we can simplify it further by restricting the set of values of the angles in (10) from the whole interval  $[0, 2\pi)$  to a discrete set of three values separated by  $2\pi/3$ , for instance,  $\pi/3, \pi, 5\pi/3$ . For this choice, the first vector  $e_1$  of a frame at a triangle points from the center of the triangle to one of its vertices. In a sense, this set of three frame positions is a minimal set reflecting the symmetry of equilateral triangle.

Since physical quantities do not depend on the choice of frames, this restriction is a sort of gauge condition. With this choice, the blocks (10) may admit only nine different forms depending on the nine different choices of the angles  $\phi_i^j, \phi_j^i$  in (10). They can be precomputed. For example, for the frame assignment in fig.1  $\phi_i^{(j)} = 5\pi/3, \phi_j^{(i)} = \pi$  and for  $s_{ij} = 1$  we have

$$\mathcal{H}_{ij} = \begin{pmatrix} -\frac{\sqrt{3}}{2} & \frac{1}{2} \\ 0 & 0 \end{pmatrix}, \quad \mathcal{H}_{ji} = \begin{pmatrix} 0 & -\frac{1}{2} \\ 0 & -\frac{\sqrt{3}}{2} \end{pmatrix}. \quad (13)$$

## Fermions and the Ising model

The idea is now to calculate spectra of the Dirac-Wilson operator for different triangulations from the ensemble (1). Summing up (averaging) all the spectra we obtain the spectrum of the Dirac-Wilson operator for fermions interacting with 2d gravity. More precisely, we will consider a field of Majorana-fermions coupled to gravity. At the critical point it corresponds to the conformal field with the central charge  $c = 1/2$ .

Denote the components of the spinor  $\Psi$  by  $\Psi_\alpha$ , and of  $\bar{\Psi}$  by  $\Psi^\beta$ . The Majorana condition reads :  $\Psi^\beta = \epsilon^{\beta\alpha}\Psi_\alpha$  or  $\Psi_\alpha = \Psi^\beta\epsilon_{\beta\alpha}$ , where  $\epsilon$  is the standard antisymmetric tensor, In this notation, the action for Majorana fermions can be written as

$$S_T = \sum_{ij} \Psi_i^\alpha [\mathcal{D}_{ij}]_\alpha^\beta \Psi_{j\beta} = \sum_{ij} \Psi_{i\alpha} \widehat{\mathcal{D}}_{ij}^{\alpha\beta} \Psi_{j\beta}, \quad (14)$$

where

$$\widehat{\mathcal{D}}_{ij}^{\alpha\beta} = \epsilon^{\alpha\gamma} [\mathcal{D}_{ij}]_\gamma^\beta = \frac{1}{2} \epsilon^{\alpha\beta} \delta_{ij} - K P_{ij} \epsilon^{\alpha\gamma} [\mathcal{H}_{ij}]_\gamma^\beta, \quad (15)$$

or in short  $\widehat{\mathcal{D}} = \epsilon \mathcal{D}$  :

$$\widehat{\mathcal{D}} = \widehat{\mathcal{D}}_0 - K \widehat{\mathcal{H}} \quad (16)$$

where  $\widehat{\mathcal{D}}_0 = \frac{1}{2}\epsilon \times \mathbb{1}$  is a deterministic part, and  $\widehat{\mathcal{H}}$  is a random part which consists of two-by-two matrices  $\widehat{\mathcal{H}}_{ij} = \epsilon \mathcal{H}_{ij}$  (10) located at nonvanishing positions of the adjacency matrix  $P_{ij}$  which correspond to pairs of neighboring triangles.  $P_{ij}$  is an off-diagonal random matrix in the  $ij$  indices.

One can show that  $\widehat{\mathcal{D}}$  is antisymmetric under the change of pairs of indices

$$\widehat{\mathcal{D}}_{ij}^{\alpha\beta} = -\widehat{\mathcal{D}}_{ji}^{\beta\alpha}, \quad (17)$$

and hence  $\text{Pf}^2 \widehat{\mathcal{D}} = \text{Det} \widehat{\mathcal{D}} = \text{Det} \mathcal{D}$ . For each triangulation individually, the integral over fermions in (1) yields Pfaffian of the matrix  $\widehat{\mathcal{D}}$ . Thus for Majorana fermions on a two-dimensional triangulation the partition function (1) is a sum of Pfaffians of the Dirac-Wilson operator

$$\mathcal{Z} = \sum_{T \in \mathcal{T}} \mathcal{Z}_T = \sum_{T \in \mathcal{T}} \text{Pf} \widehat{\mathcal{D}}_T = \sum_{T \in \mathcal{T}} \text{Det}^{1/2} \mathcal{D}_T. \quad (18)$$

In the last step we have used the inequality  $\text{Pf} \mathcal{D}_T > 0$ , which can be proven by the hopping parameter expansion. The consistency condition (8) turns out to be essential in the proof. Namely, one shows that the Pfaffian is represented as a sum over loop configurations each of which contributes a positive factor if the condition (8) is met [13, 14].

Using this expansion one can also establish the equivalence between the partition function  $\mathcal{Z}_T$  and the partition function of the nearest neighbor Ising model with spins  $\sigma_{i_*}$  located at the vertices  $i_*$  of  $T$

$$Z_T = \sum_{\{\sigma_*\}_T} e^{-\beta E_T} \quad (19)$$

where

$$E_T = - \sum_{(i_* j_*) \in T} (\sigma_{i_*} \sigma_{j_*} - 1). \quad (20)$$

The partition functions  $Z_T$  (19) and  $\mathcal{Z}_T$  (1) are equal for

$$K = \frac{e^{-2\beta}}{\sqrt{3}}. \quad (21)$$

In the derivation of this equivalence one identifies loop configurations, arising in the hopping expansion of  $\mathcal{Z}_T$  with domain walls of the Ising model. Again,



the consistency condition (8) plays the crucial role here. For a non-spherical triangulation one has to carefully treat topological effects related to the existence of non-contractable loops which may give a negative contribution for antiperiodic boundary conditions. One can get rid of all negative contributions performing the GSO projection that is summing over all spin structures of the manifold [21]. This and another topological issues are discussed elsewhere [14]. Here we will restrict ourselves to spherical triangulations for which we automatically have  $\mathcal{Z}_T = Z_T$  for each triangulation  $T \in \mathcal{T}$  and hence also for the sum over all triangulations in  $\mathcal{T}$

$$\mathcal{Z} = Z \equiv \sum_{T \in \mathcal{T}} Z_T. \quad (22)$$

The critical temperature of the Ising model for the partition function  $Z$  is known analytically to be  $\beta = \frac{1}{2} \ln \frac{131}{85} \approx 0.2162730$  [17]. Translating the critical temperature to the hopping parameter (21) we obtain the following critical value

$$K_{cr} = \frac{85\sqrt{3}}{393} \approx 0.3746166 \quad (23)$$

for which fermions become massless. Another interesting point which can be deduced from the equation (21) is that the value of the hopping parameter  $K_0 = 1/\sqrt{3}$  corresponds to  $\beta = 0$  which is the border between the ferromagnetic and antiferromagnetic regimes. For  $\beta < 0$  one expects frustration in the Ising model on a triangulation and hence that the lowest energy state is highly degenerated. As we will see below, the behavior of the spectrum of the Dirac-Wilson is also sensitive to passing over this border. First, we will however restrict  $K$  to the 'ferromagnetic' range  $[0, K_0]$ .

The equivalence of the partition functions  $Z_T$  and  $\mathcal{Z}_T$  may be used to relate the average energy  $\overline{E}_T$  of the Ising model on a triangulation  $T$  to eigenvalues of the Dirac-Wilson operator. Differentiating both sides of (18) with respect to  $\beta$  we obtain

$$\overline{e}_T = \frac{\overline{E}_T}{N} = -\frac{1}{N} \frac{\partial}{\partial \beta} \ln Z_T = 1 - \frac{\sum_a \lambda_a^{-1}}{2N}, \quad (24)$$

where  $\lambda_a$  are eigenvalues of the Dirac-Wilson operator  $\mathcal{D}_T$ . For our choice of the representation of gamma matrices,  $\mathcal{D}_T$  is a real matrix. Its spectrum consists of either real eigenvalues or of pairs of complex conjugates. Thus the sum on the right hand side of (24) is a real number. Similarly, the fluctuations of the Ising energy on the triangulation  $T$  are given by

$$\sigma_T^2 = \frac{\overline{E}_T^2 - \overline{E}_T^2}{N} = \frac{1}{N} \frac{\partial^2}{\partial \beta^2} \ln Z_T = -\frac{\sum_a \lambda_a^{-2}}{2N} + \frac{\sum_a \lambda_a^{-1}}{N}. \quad (25)$$

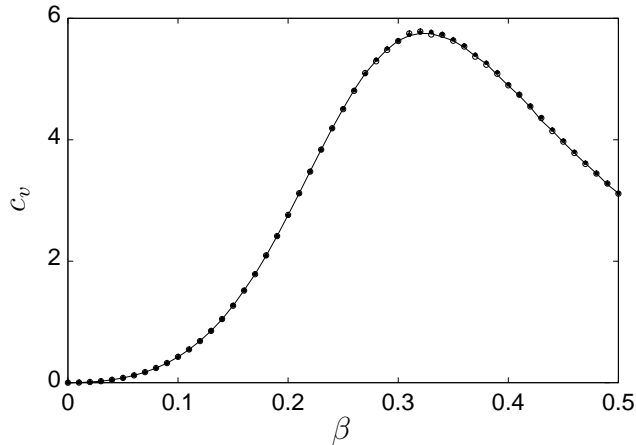


Figure 2: Heat capacity  $c_v(\beta)$  for the system with  $N = 16$  triangles for the three cases discussed in the text : (a) ising-ising (line); (b) ising-fermion (filled symbols); (c) fermion-fermion (empty symbols). The three methods give the same results within the error bars, which are here of order of the size of the symbols used.

Averaging over triangulations we obtain the energy density and heat-capacity of the Ising model coupled to gravity calculated in terms of the eigenvalues of the Dirac-Wilson operator

$$e = \langle \bar{e}_T \rangle = 1 - \left\langle \frac{1}{2N} \sum_a \lambda_a^{-1} \right\rangle, \quad (26)$$

$$c_v = \beta^2 \langle \sigma_T^2 \rangle = \beta^2 \left\{ - \left\langle \frac{1}{2N} \sum_a \lambda_a^{-2} \right\rangle + \left\langle \frac{1}{N} \sum_a \lambda_a^{-1} \right\rangle \right\}. \quad (27)$$

The equivalence of the models can also be very useful in MC simulations of the model. To show this, let us compare three numerical experiments in which (a) the Ising model is used to generate triangulations and to measure the Ising energy and heat capacity; (b) the Ising model is used as a generator of triangulations but measurements are carried out using the fermion field; (c) the fermionic model is used both to generate triangulations and to perform measurements. As shown in fig.2 the three methods yield exactly the same results. The methods differ, however, significantly in the CPU time needed to generate results of the same quality. The first difference comes from the configuration generator which is much faster for the Ising model than for the fermionic determinant. In the latter case, to calculate a Metropolis weight

for a single local change of triangulation, *i.e.* a flip of one link on the triangulation, requires the recomputation of the determinant of the Dirac-Wilson operator on the modified lattice. This is a tedious task for which the number of operations grows with the third power of the system size  $N$ . Thus one expects that the time of a sweep through the lattice grows as  $N^4$  for the fermionic configurations generator. One sweep for the Ising model, which consists of a sweep of local updates of Ising spins, a fixed number of Wolff cluster updates, and a sweep of local changes of triangulation, lasts in CPU units roughly proportionally to the system size  $N$ . Thus, the fermionic algorithm is competitive with the Ising generator only for very small lattices. As far as measurements are concerned the situation is more complex. For example, one cannot determine the spectrum of the Dirac-Wilson operator using only the Ising spins. One can, however, do the opposite. For a given lattice, the time of calculating all eigenvalues of the Dirac-Wilson operator is proportional to  $N^3$ . Having done this, one is able for this triangulation to exactly calculate the Ising energy (24) and its higher moments (25) without statistical fluctuations. If one instead used the Ising model, one has to sample Ising configuration many times to reduce the error. In general, the cost of a single measurement of the energy is proportional to  $N$ . The error of the single measurement of the energy density decreases like  $1/\sqrt{N}$ . Summarizing, we expect the CPU time to measure energy with a given precision to grow as  $\sqrt{N}$ . The CPU time grows rapidly with the order for measurements of higher moments of energy.

In order to obtain the data the quality presented in fig. 2 for  $N = 16$ , the methods discussed above required (a) 1000 CPU min. (b) 6 CPU min. and (c) 100 min. on the computer Alpha XP1000/EV6/500 MHz.

## Spectrum of the Dirac-Wilson operator

In the production runs we use the method (b), which relies on generating triangulations from the partition function of the Ising model. At each measurement we ignore the values of the Ising spins and we assign frames  $e_i$  and  $s_{ij}$ -signs to the triangulation to reconstruct the Dirac-Wilson operator (10,11).

A typical spectrum of the Dirac-Wilson operator on random triangulation is shown in fig.3. The main effect on the spectrum of changing the hopping parameter  $K$  is to rescale it around the point  $(\frac{1}{2}, 0)$ . The positions of the two claw-shaped ends of the spectrum move with  $K$ . One can find a value of  $K$  for which the ends lie closest to the origin  $(0, 0)$ . This value can be treated as a pseudo-critical value  $K_*$  for which the mass of the fermion excitation

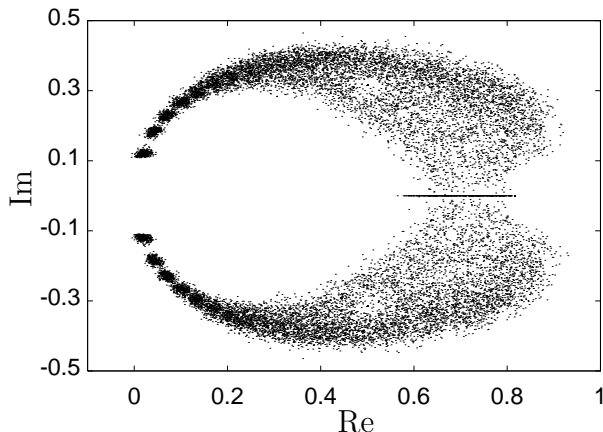


Figure 3: The distribution of eigenvalues  $\lambda$  of the Dirac-Wilson operator for  $N = 64$  and  $K = 0.364$  on random lattice.

is minimal. For  $K < K_*$  the origin  $(0, 0)$  lies outside the claws, while for  $K > K_*$  inside. In fact, this is the main difference between the two regimes, since beside the scaling factor the shape of the spectrum is almost constant.

The claw-shaped ends of the pseudo-critical spectra successively approach each other when the system size  $N$  is increased. They eventually close entirely at the origin  $(0, 0)$  for infinite  $N$ , signaling the occurrence of massless excitations.

One can alternatively study the spectrum of the operator  $\widehat{\mathcal{D}} = \epsilon \mathcal{D}$ . In fact, this operator is closer related, in spirit, to Majorana fermions (15) due to the presence of the charge conjugation matrix  $\epsilon$ . Since the matrix  $\widehat{\mathcal{D}}$  is antisymmetric, and it is real in our representation, its spectrum is purely imaginary. Thus, the eigenvalue density of this operator is one dimensional :

$$\widehat{\rho}(x) = \lim_{N \rightarrow \infty} \frac{1}{N} \left\langle \sum_{\widehat{\lambda}} \delta(x - i\widehat{\lambda}) \right\rangle. \quad (28)$$

The spectrum is symmetric  $\widehat{\rho}(x) = \widehat{\rho}(-x)$ . We will constrain ourselves to the positive branch. For each triangulation eigenvalues of the positive part of the spectrum can be ordered :  $\lambda_0 \leq \lambda_1 \leq \lambda_2 \leq \dots$ . Collecting separately histograms for the lowest, second lowest, third lowest eigenvalues *e.t.c.* one obtains distributions  $\widehat{\rho}_j(x)$  of the  $j$ -th eigenvalue. Of course, by construction :  $\widehat{\rho}(x) = \sum_j \widehat{\rho}_j(x)$ .

We studied numerically the dependence of  $\widehat{\rho}_j(x)$  on the hopping parameter. In figure 4 is shown the distribution  $\widehat{\rho}_0(x)$  for different values of  $K$ . One can see that it is discrete for  $K_0 = 1/\sqrt{3}$  consisting of separate nar-

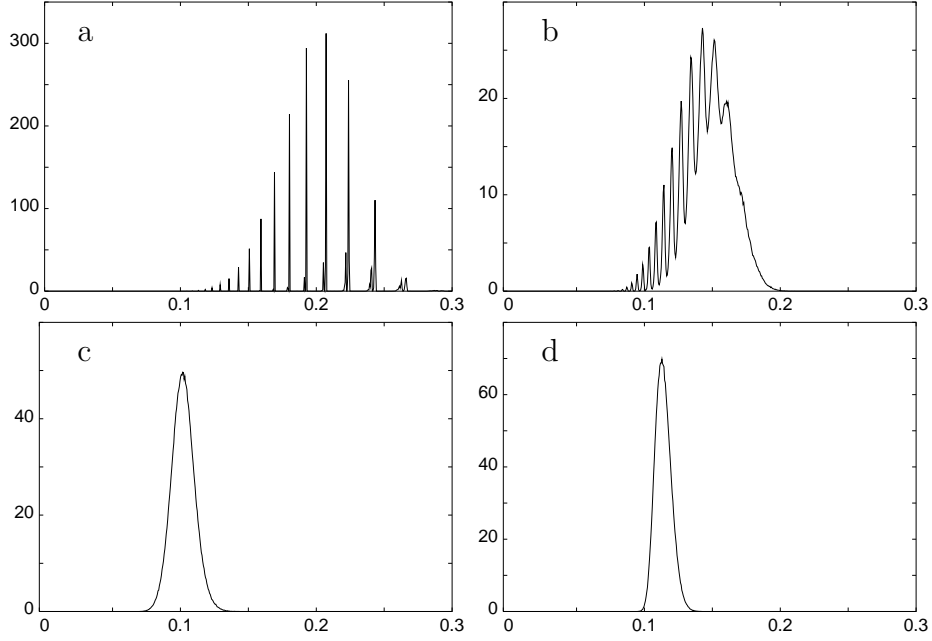


Figure 4: Evolution of the shape of the probability distribution  $\widehat{\rho}_0(x)$  of the lowest eigenvalue of the operator  $\epsilon\mathcal{D}$  for  $N = 64$  as a function of the hopping parameter  $K$  : (a)  $K = 1/\sqrt{3} = 0.5774$ , (b)  $K = 1/\sqrt{3}e^{-0.2} = 0.4727$ , (c)  $K = 1/\sqrt{3}e^{-0.4} = 0.3870$ , (d)  $K = 1/\sqrt{3}e^{-0.6} = 0.3169$ . Each histogram presented in the figure contains  $7 \times 10^5$  counts. The bin size is  $5 \times 10^{-4}$ . The histograms are normalized to have area one.

row peaks. This may appear surprising at first glance. However, when  $K$  becomes smaller than  $K_0$  this spectrum becomes continuous : it gradually changes when  $\Delta = K_0 - K$  grows to eventually become a smooth bell-shaped distribution (fig.4). As we shall see below the discreteness of the spectrum at  $K_0 = 1/\sqrt{3}$  is not a finite size effect. We made the following experiment. We generated a quenched ensemble of random triangulations by ignoring the coupling of fermions to gravity. It is an ensemble of triangulations for pure gravity. Then, for each triangulation from this ensemble, we calculated the operator (15) and determined its lowest eigenvalues for different values of  $K$ . One can expect that outside the critical region, where fermions are massive, the approximation should not significantly affect the spectrum of the model. Indeed we checked numerically for a few values of  $K$  that it is practically impossible to distinguish between the spectrum for the quenched and the full model.

The results of the quenched experiment are presented in figure 5 where

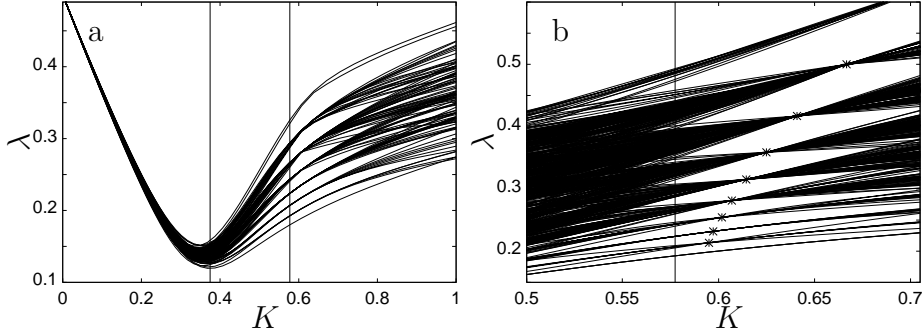


Figure 5: (a) Evolution of the lowest eigenvalue of the operator (15) with the hopping term, calculated on an ensemble of given triangulations with  $N = 32$  triangles. (b) Evolution of seven lowest eigenvalues of the operator (15). The cross-points of the bundles in the 'antiferromagnetic' phase are seen. The cross-points can be numbered by successive integers from 6 to 13 corresponding to the length  $q$  of the elementary loops, as discussed in the text.

one can see lowest eigenvalues of the operator (15) for different  $K$ . The 'ferromagnetic' region corresponds to the interval  $0 \leq K < 1/\sqrt{3} = 0.5774$ , and the 'antiferromagnetic' one  $K > 1/\sqrt{3}$ . Universal properties of the model are encoded in the behavior of the spectrum around the critical value  $K_{cr} = 0.3746$  (23), lying deep inside the 'ferromagnetic' phase, where the eigenvalue bundle has a dip. For  $K \rightarrow 0$  only the deterministic part  $\frac{1}{2}\epsilon^{\alpha\beta}\delta_{ij}$  of the operator (15) survives.

The bundles of eigenvalues have an interesting property, The lines of the bundle cross at some points in the 'antiferromagnetic' phase (see fig. 5). The meaning of a cross-point is that, for the corresponding value of  $K$ , the operator (15) has a common identical eigenvalue for many different triangulations. The reason why it happens is that this eigenvalue is entirely related to the existence of elementary loops of the length  $q$  on the triangulation and not to the whole random structure of the triangulation, as it generically takes place.

In order to understand the mechanism of the occurrence of the cross-points, consider an elementary loop on the dual lattice of length  $q$  consisting of vertices  $i_1, i_2, \dots, i_q$ . One can show that the corresponding submatrix  $2q \times 2q$  of (15) built of the two-by-two blocks at the  $(i_1, i_2, \dots, i_q) \times (i_1, i_2, \dots, i_q)$  positions has for some  $K_q$  an eigenvalue  $\lambda_q$  which depends only on  $q$ . The pair  $(K_q, \lambda_q)$  corresponds to a cross-point in the figure (5). Furthermore, it turns out that for  $K = K_q$  and  $\lambda = \lambda_q$  the entire  $2q$  rows for  $i_1, i_2, \dots, i_q$

of the matrix  $\widehat{\mathcal{D}} - \lambda_q \mathbb{1}$  are linearly dependent. This means that  $\lambda_q$  is not an eigenvalue of the submatrix but also of the whole matrix  $\widehat{\mathcal{D}}$  for  $K = K_q$  (15). The pairs  $(K_q, \lambda_q)$  correspond to the cross-points of eigenvalues bundles in fig. 5. They can be numbered by  $q$ . We found  $(K_q, \lambda_q)$  to be  $(2/\sqrt{3}, 3/2)$ ,  $(\sqrt{2}/\sqrt{3}, \sqrt{3}/2)$ ,  $((\sqrt{5} - 1)/\sqrt{3}, \sqrt{15 - 6\sqrt{5}}/2)$ ,  $(2/3, 1/2)$  for  $q = 3, 4, 5, 6$ , respectively. Positions of the cross-points do not change with the lattice size. This structure of the cross-points will be discussed in more detail elsewhere. Here we only want to mention some features of this structure. All the points lie in 'antiferromagnetic' phase. It is seen in fig.5 that for  $q \rightarrow \infty$  the points approach the border to the 'ferromagnetic' phase  $K_q \rightarrow K_0$  and that the corresponding eigenvalues  $\lambda_q$  decrease. Moreover the probability of encountering an elementary loop of length  $q$  on random triangulation falls off exponentially [2] which means that there are very few loops with high  $q$ . Taking all these facts into account one may expect that the presence of discrete line of cross-points which approaches  $K_0$  shall dominate the shape of the spectra for the lowest eigenvalues at  $K_0$ , leading in particular to the appearance of discrete peaks also in the limit  $N \rightarrow \infty$ .

On the other hand, one also expects that the discreteness of the spectrum disappears when  $K$  goes deeper into the ferromagnetic phase. The crossover between the two regimes depends on some combination of  $\Delta K = K_0 - K$  and the system size  $N$ . For  $\Delta K$  larger than zero, indeed the amplitude of the fluctuations decreases with the size as can be seen in fig.6. The fluctuations disappear in the limit  $N \rightarrow \infty$  leaving out a smooth distribution.

The spectra  $\widehat{\rho}_j(x)$  of other eigenvalues  $\lambda_j$ ,  $j > 0$ , also exhibit the same fluctuating pattern at  $K_0$  as for  $j = 0$ , however the amplitude of the fluctuations decreases faster with  $\Delta K$  and  $N$ . As one can, for example, see in fig.7.c the oscillations are absent in the spectrum of the third lowest eigenvalue  $\rho_2(x)$  already for  $K = 0.4727$ .

For  $K$  far from  $1/\sqrt{3}$  density distributions are smooth. In this case, the situation resembles the one known for instance from the considerations of chiral matrix models : separate densities  $\widehat{\rho}_j(x)$  are described by bell-shaped functions [29]. They sum up  $\widehat{\rho}(x) = \sum_j \widehat{\rho}_j(x)$  to a function with oscillations [27] like for example in fig.7.d. It would be interesting to find a random matrix model which reproduces  $\widehat{\rho}_j(x)$  and  $\widehat{\rho}(x)$  analytically.

Another interesting feature of the histograms is the presence of singular peaks for which the number of entries grow with the size of the lattice. The peaks lie outside the range displayed in the figures. We show in the appendix that such peaks are also present in the spectrum on the regular lattice. In this case we calculated analytically that the height of the peaks is logarithmically divergent in the lattice size. Thus this seems to be a generic situation.

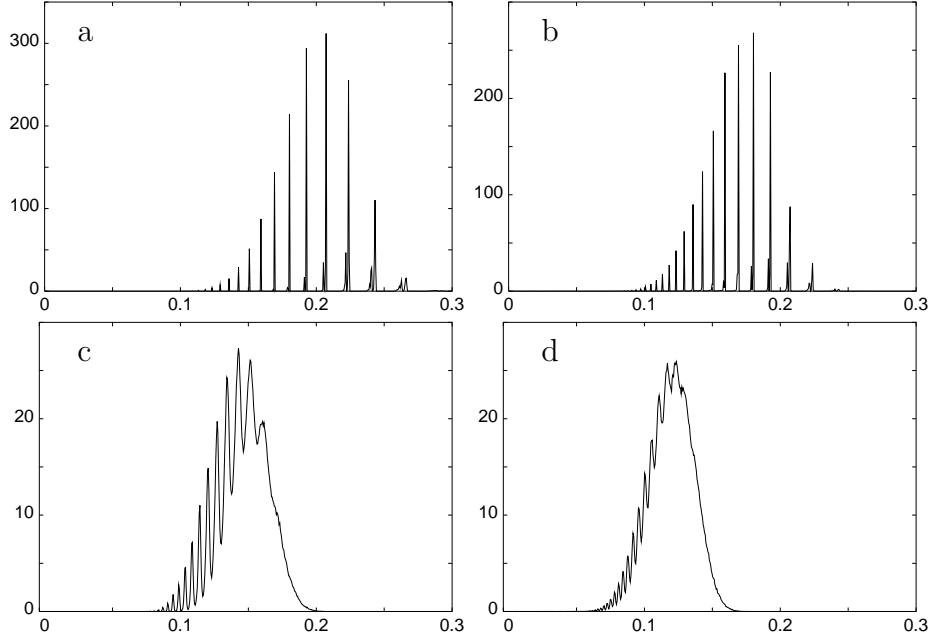


Figure 6: The probability distribution  $\hat{\rho}_0(x)$  for (a)  $K_0 = 1/\sqrt{3}$ ,  $N = 64$ , (b)  $K_0 = 1/\sqrt{3}$ ,  $N = 128$ . (c)  $K = 1/\sqrt{3}e^{-0.2} = 0.4727$ ,  $N = 64$  (d)  $K = 1/\sqrt{3}e^{-0.2} = 0.4727$ ,  $N = 128$ . The amplitude of the oscillations in the bottom row decreases with  $N$ . The histograms (a) and (b) contain  $2 \times 10^5$  counts each, (c)  $6 \times 10^5$ , (d)  $7 \times 10^5$ . The bin size is  $5 \times 10^{-4}$ .

Let us come back to the universal properties of the system of fermions interacting with gravity. We will study now in more detail behavior of the spectrum at the critical point of the Ising model. More precisely we shall be interested in the mass gap of the of the spectrum at  $K$  close to  $K_{cr}$ . We define the gap as the position of the center of mass for the distribution of the lowest eigenvalue  $\hat{\rho}_0(x)$ . We denote it by  $M = \int x \hat{\rho}_0(x)$ . We want to determine the dependence  $M = M(K)$  on the hopping parameter  $K$  for the given system size  $N$ . We do this numerically using the Lanczos algorithm<sup>2</sup>.

<sup>2</sup>The Lanczos algorithm [22] is an iterative procedure to calculate eigenvalues. It is frequently used to approximately determine the lowest part of the eigenvalue spectra of large matrices, for which exact standard diagonalization algorithms would require a too long time. In a single iteration step the Lanczos algorithm finds one approximated eigenvalue and improves quality of the previously calculated ones. As a rule it first produces the smallest and the largest eigenvalues and then successively fills up the remaining part of the spectrum, The accuracy increases with the number of iterations. We checked in our case using matrices of sizes up to 128, that when we keep the number  $n$  of iteration proportional to the size of the matrix  $n = cN$  with,  $c = 0.25$ , the distribution of the lowest



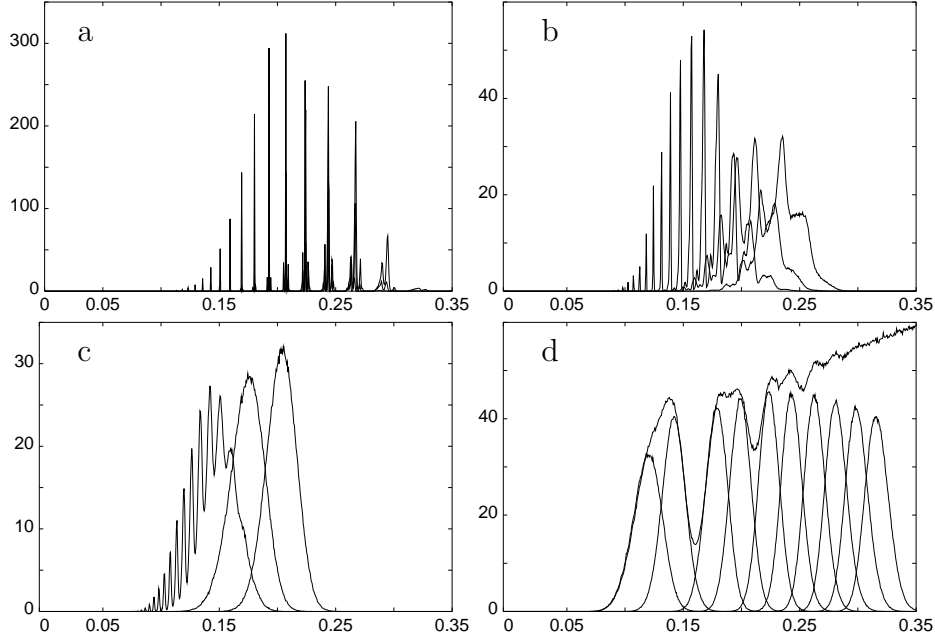


Figure 7: The figures show probability distributions  $\hat{\rho}_j(x)$  of the lowest eigenvalues for  $N = 64$  and (a)  $K = 1/\sqrt{3} = 0.5774$ , (b)  $K = 1/\sqrt{3}e^{-0.1} = 0.5224$ , (c)  $K = 1/\sqrt{3}e^{-0.2} = 0.4727$ , (d)  $K = 1/\sqrt{3}e^{-0.3} = 0.4277$ . More precisely, each figure (a-c) contain distributions for  $j = 0, 1, 2$ , while the figure (d) for  $j = 0, 1, \dots, 9$ . Additionally, in the figure (d) the p.d.f.  $\hat{\rho}(x)$  is shown. Each histogram  $\hat{\rho}_j(x)$  contains  $6 \times 10^5$  counts and has the bin size is  $5 \times 10^{-4}$ , while  $\rho(x)$  contains  $10^6$  counts, and has the bin size  $1.25 \times 10^{-3}$ .

For given  $N$  the function  $M(K)$  has a minimum (see fig.8). The value of the minimum  $M_*$  plays the role of a mass gap, while its position  $K_*$  of a pseudo-critical hopping parameter. We determined  $K_*$  and  $M_*$  for different system sizes. The results are collected in the table 1. We fitted the data points to the following finite size scaling formulas

$$M_* = \frac{b}{N^{\frac{1}{d_H}}} \left( 1 + \frac{t}{N} \right) \quad , \quad K_* = K_\infty - \frac{a}{N^\kappa} . \quad (29)$$

The exponent  $d_H$  is the fractal dimension of the surface given. A typical linear extent of  $L$  scales as  $L = N^{1/d_H}$ . When the physical mass is equal zero,  $L$  sets the scale for the correlation length. Its inverse gives the minimal eigenvalue of the spectrum  $M_*$ . For smaller systems one expects corrections to scaling. We took it into account by introducing a phenomenological eigenvalue agrees with the one obtained by an exact algorithm.

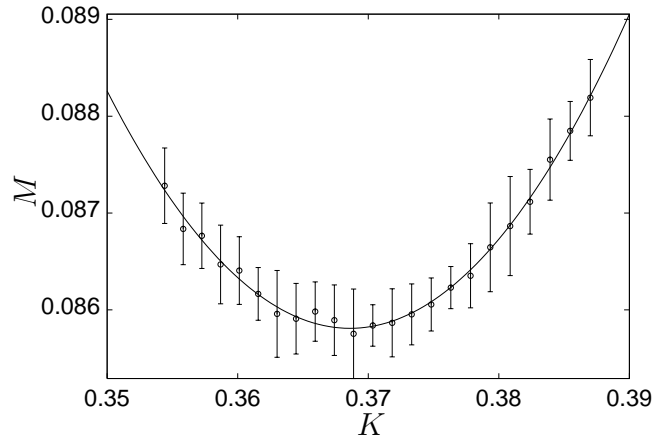


Figure 8: The position of the center of mass is shown for the distribution of the smallest eigenvalue of the operator  $\widehat{\mathcal{D}}$  for  $N = 96$  as a function of the hopping parameter  $K$ .

$N$	$K_*$	$M_*$
32	0.352(3)	0.1395(5)
48	0.360(2)	0.1162(4)
64	0.364(2)	0.1016(2)
96	0.368(2)	0.0858(2)
128	0.370(1)	0.0766(2)
192	0.372(2)	0.0656(3)
256	0.372(2)	0.0589(3)
384	0.374(2)	0.0509(3)
512	0.374(2)	0.0459(4)
768	0.375(3)	0.0397(2)
1024	0.375(1)	0.0359(3)

Table 1: Positions and values of the minima of the function  $M(K)$  representing the center of mass of the distribution of the smallest eigenvalue of the operator  $\widehat{\mathcal{D}}$  for different system sizes  $N$ .

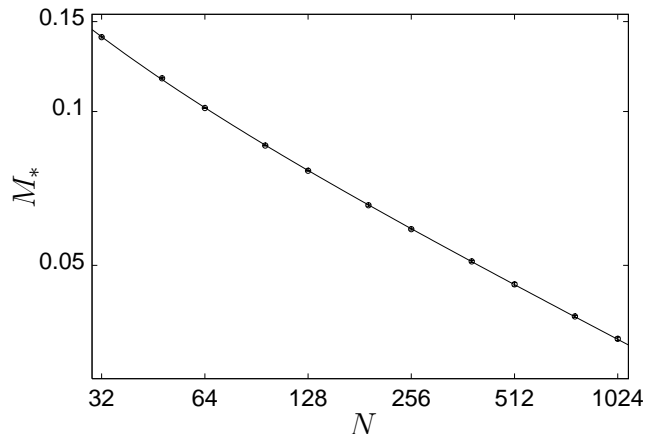


Figure 9: The mass gap  $M_*$  for different system sizes  $N$ , and the curve representing the best fit to the formula (29) :  $1/d_H = 0.348(4)$ ,  $b = 0.40(1)$  and  $t = 5.7(5)$ .

correction  $t/N$  to the formula (29). This correction significantly improves quality of the fit for the studied range of  $N$ . The best fit to the formula is  $1/d_H = 0.348(4)$ ,  $b = 0.40(1)$  and  $t = 5.7(5)$ . The corresponding curve is plotted in fig.9. The curve fits indeed very well to all the data points. The error bars of the best fit parameters were estimated by jack-knife.

We compared the goodness of the best fits to the formula (29) and analogous formulas in which the correction  $t/N$  was substituted by  $t/N^{1/2}$  and  $t/N^{3/2}$ . We obtained  $\chi^2/\text{d.o.f.} = 0.52$  for  $t/N$  while in the other two cases 1.66 and 1.83, respectively. Thus, among those three correction types, the one  $t/N$  is best in this range. We have also checked that the fitted value  $1/d_H = 0.348(4)$  is stable against the successive removal of the data points of the smallest volumes.

There are different theoretical predictions for the value of the Hausdorff dimension  $d_H = 4$  [23, 24] and  $d_H = 3$  [25], the latter of which was obtained for a test fermion in the gravitational background coupled to matter field with the central charge  $c = 1/2$  [25]. The Hausdorff dimension measured in our MC simulations  $d_H = 2.87(3)$  favors  $d_H = 3$ . One should, however, be aware that in measurements of the Hausdorff dimension there are large finite size effects, as can be seen from the considerations of pure gravity [23].

The best fit for the second formula in (29) is given by  $K_\infty = 0.3756(16)$ ,  $\kappa = 1.03(30)$  and  $a = 0.9(5)$  (see fig.10). The limiting value  $K_\infty$  is in agreement with the theoretically calculated critical value  $K_{cr}$  (23). The scaling exponent  $\kappa$  is almost equal 1 which would suggest a kinematic scaling saying

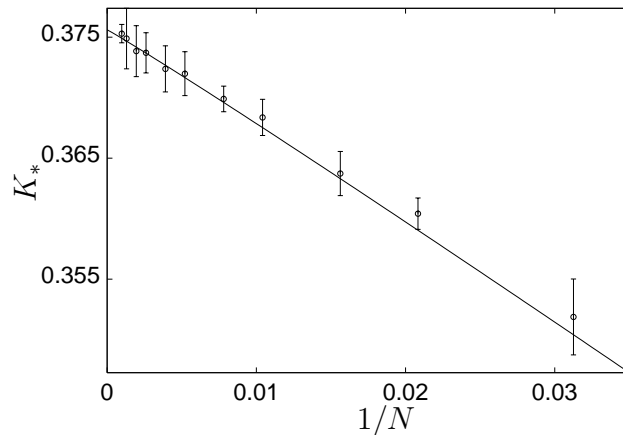


Figure 10: The pseudo-critical parameter  $K_*$  for different system sizes  $N$ , and the curve representing the best fit to the scaling formula (29) :  $K_\infty = 0.3756(16)$ ,  $\kappa = 1.03(30)$   $a = -0.9(5)$ , plotted as a function of  $1/N$ .

that the average distance between eigenvalues decreases as  $1/N$ .

## Conclusions and outlook

We have investigated the properties of the Dirac-Wilson operator on a random triangulation. In particular we have extracted from the spectrum of the operator the values of the fractal dimension  $d_H$  and the critical value of the hopping parameter  $K_{cr}$ . At this value of  $K = K_{cr}$  the fermions become massless and one can take a continuum limit corresponding to massless fermions interacting with  $2d$  gravity. The value of  $K_{cr}$  has been calculated analytically, however,  $d_H$  has not been unambiguously determined theoretically. In the neighborhood of  $K_{cr}$ , which lies deep in the ferromagnetic phase we found spectral distributions which are typical for random systems.

Apart from  $K_{cr}$  there is another interesting value of  $K$ , namely  $K_0 = 1/\sqrt{3}$  which lies on the border between the ferromagnetic and antiferromagnetic phases of the corresponding Ising model. We observed that the distributions of the lowest eigenvalues,  $\hat{\rho}_j(x)$ , becomes discrete when  $K$  goes to  $K_0$  from below. This is an unexpected phenomenon for a random system.

For some values of the hopping parameter  $K$  in the 'antiferromagnetic' phase, eigenvalues of the Dirac-Wilson operator decouple from the random structure of the matrix and depend only on local geometrical properties of the triangulation. This, as we discussed, leads to the appearance of discrete spectra at  $K_0$ .

There are many natural extensions of the studies presented in this work. One should try to understand properties of the spectrum of the Dirac operator from the point of view of the random matrix theory [26, 27, 28]. This is a slightly different type of randomness than the one provided by the coupling to the vector gauge field which is usually discussed in the context of QCD. However exactly this type of randomness may be important in quantum gravity.

Next, one can investigate in more detail the relation of the quenched approximation to the full model. The quenched model describes a test particle in pure gravity. From this exercise one could perhaps draw a general lesson about the effect of quenching on the spectrum of the Dirac operator. This can be important because this type of approximation is frequently used in many physical contexts, for example, in QCD. However, one usually is not able to quantify the effects of quenching.

Furthermore, one can study effects of changing topology by considering non-spherical 2d-triangulations. As mentioned, this requires a careful treatment of various spin structures which may be admitted by a manifold. Contrary to higher dimensional case, where the existence of spin structure is related to the second Stiefel-Whitney class [20], here the question of the existence reduces to the orientability of the manifold. Also the classification of spin structures is relatively simple in the 2d case. The spin structures can be classified by a set of signs defined on all classes of non-contractable loops. The signs tell us whether boundary conditions for a parallel transport of a spinor around those loops are periodic (+1) or anti-periodic (-1). For a manifold with genus  $h$ , there are  $2h$  different classes of non-contractable loops and hence there are  $2^{2h}$  different spin structures.

Finally one should try to find a lattice implementation of the Dirac operator for higher dimensional compact simplicial manifolds. Many parts of the construction can be directly generalized from the 2d case; actually almost all, except the link sign degrees of freedom,  $s_{ij}$  (9), which as it turns out are not sufficient in general case for the connections  $\mathcal{U}_{ij}$  to fulfill the consistency condition for all plaquettes (8).

## Acknowledgments

We thank J. Jurkiewicz, A. Krzywicki, E. Laermann, D. E. Miller and J. Tabaczek for many discussions. This work was supported in part by the EC IHP grant HPRN-CT-1999-00161 and by the Polish Government Project (KBN) 2P03B 01917. At the first stage of this work L.B. was supported by a DAAD fellowship.

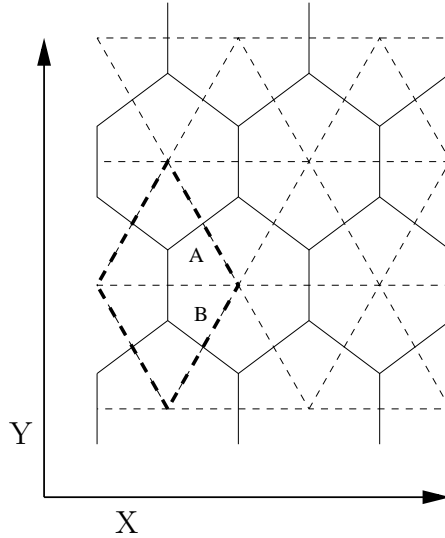


Figure 11: Regular triangulation of the plane and its dual lattice. Fermions live on the vertices of the dual (honey-comb) lattice. The elementary cell contains two distinct dual node positions denoted by  $A$  and  $B$ .

## Appendix

For a comparison in the appendix we calculate spectrum of the Dirac-Wilson operator on the regular planar triangulation built of equilateral triangles with fermion field located in the centers of triangles. If one connects the centers by links, they form a dual lattice; in this case it is a honey-comb lattice (see fig.11). It is convenient to divide the vertices of this lattice into two classes  $A$  and  $B$  forming a check-board. The fundamental cell on the triangulation contains one site of each. One reconstructs the entire triangulation translationally copying the fundamental cell using multiples of two the vectors  $d_1 = n_0 + n_1$ , and  $d_2 = n_0 + n_2$  constructed from the link vectors  $n_0 = (0, 1)$ ,  $n_1 = (\sqrt{3}/2, 1/2)$ ,  $n_2 = (-\sqrt{3}/2, 1/2)$ .

Using translational symmetry of the lattice we can now rewrite the action

(2) in the following form

$$\begin{aligned}
S &= -\frac{K}{2} \sum_i \sum_{d=1}^2 [\bar{\psi}_{i+d,A}(1+n_d \cdot \gamma)\psi_{i,B} + \bar{\psi}_{i,B}(1-n_d \cdot \gamma)\psi_{i+d,A}] \\
&\quad -\frac{K}{2} \sum_i [\bar{\psi}_{i,A}(1-n_0 \cdot \gamma)\psi_{i,B} + \bar{\psi}_{i,B}(1+n_0 \cdot \gamma)\psi_{i,A}] \\
&\quad +\frac{1}{2} \sum_i [\bar{\psi}_{i,A}\psi_{i,A} + \bar{\psi}_{i,B}\psi_{i,B}] , \tag{30}
\end{aligned}$$

where the first index in  $\psi_{i,A}$  is a double index consisting of two integers  $(i_1, i_2)$ , which give the position of the cell  $x = i_1 d_1 + i_2 d_2$ , while the second label denotes the position A or B within the cell. In the component notation, the addition of  $d_1$  to  $i$  corresponds to  $(i_1, i_2) \rightarrow (i_1 + 1, i_2)$ , and of  $d_2$  to  $(i_1, i_2) \rightarrow (i_1, i_2 + 1)$ . In the expression (30) we have used a shorthand notation denoting the sum over  $d_1$  and  $d_2$  by  $d = 1, 2$ . We can now partially diagonalize the problem using the Fourier transform of the index  $i = (i_1, i_2)$  to the momentum space  $p = (p_1, p_2)$ . This leads us to a block-diagonal matrix consisting of four by four blocks. Each block  $D(p)$  corresponds to one Fourier mode  $\bar{\psi}_p D(p) \psi_p$ . The four by four matrix  $D(p)$  is indexed by the spinor index of  $\psi$  and of the position label A or B. For each  $p$ , diagonalization of  $D(p)$  yields four eigenvalues

$$\lambda_p = \frac{1}{2} \pm K \frac{\sqrt{3}}{2} \sqrt{w \pm i \sqrt{4 - (w - 1)^2}}, \tag{31}$$

where

$$w = \cos(p_1) + \cos(p_2) + \cos(p_1 - p_2). \tag{32}$$

The distribution of eigenvalues (31) on a finite lattice  $L \times L$  with periodic boundary condition in the  $d_{1,2}$  directions is shown in fig.12. In this case the momenta admit the values  $p_{1,2} = 2\pi k_{1,2}/L$ , where  $k_{1,2} = 0, \dots, L - 1$  and hence the operator has  $4L^2$  eigenvalues.

Similarly, one can find eigenvalues of the operator  $\hat{D}$

$$\hat{\lambda}_p = \pm \frac{i}{\sqrt{2}} \sqrt{\frac{1}{2} + \frac{K^2}{2}(w + 6) \pm \sqrt{(\frac{K^2}{2}(w - 3) + 2)^2 + 9K^2 - 4}}. \tag{33}$$

Using this formula we can calculate the spectral density

$$\hat{\rho}(x) = \lim_{L \rightarrow \infty} \frac{1}{4L^2} \sum_{\lambda} \delta(x - i\hat{\lambda}). \tag{34}$$

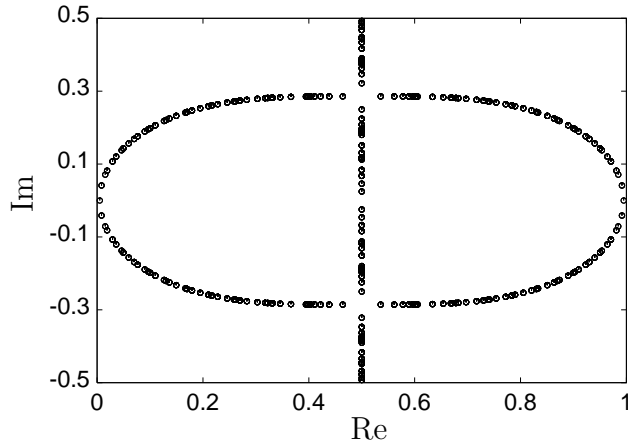


Figure 12: Eigenvalues  $\lambda$  of the Dirac-Wilson operator on a regular triangulation with  $L = 50$  and  $K = 0.33$ .

The spectrum terminates at a small positive value  $K_{cr}$  (see fig.13). It goes to zero only for  $K = K_{cr} = \frac{1}{3}$ . In the large  $L$ -limit, the two peaks in fig. 13 develop a logarithmic singularity.

For the regular lattice the critical value of the hopping parameter is given by the standard equation  $K_{cr} = 1/q$ , where  $q$  is the number of links emerging from the vertex. In this case  $q = 3$ . For random lattice this condition is dressed by lattice fluctuations. Although each vertex has coordination  $q = 3$ , the critical value of the hopping parameter is shifted from  $1/3$  to the value given by equation (23). For the regular lattice, the spectrum has an eigenvalue equal exactly zero for the critical value of the hopping parameter. This is not the case for random lattice, where the smallest eigenvalue has a distribution whose center of mass approaches zero only for large  $N$ . On the regular lattice, the lowest part of the spectrum does not move when  $N$  goes to infinity, but becomes denser. The average distance between the eigenvalues scales like  $N^{-1/d_H}$ , with the canonical dimension  $d_H = 2$  while on the random lattice, the position of the lowest eigenvalue moves towards zero with  $N^{-1/d_H}$  with a dressed exponent  $d_H = 2.87(3)$  resulting from the fractal structure of fluctuating geometry.

## References

- [1] F. David, Nucl.Phys. **B257** (1985) 45.



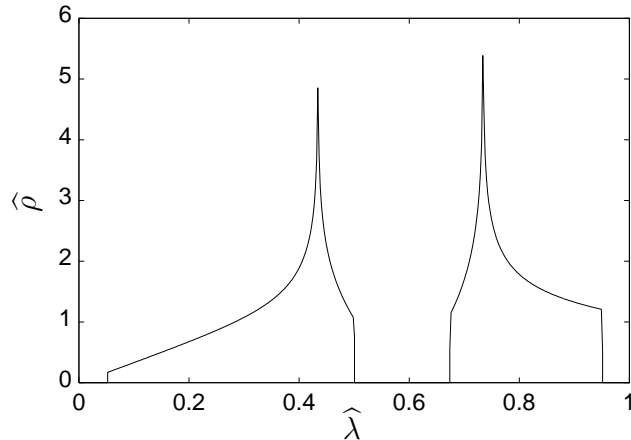


Figure 13: Histograms of eigenvalues of the operator  $\widehat{D}$  for  $L = 3000$  and  $K = 0.3$ . At the critical value  $K = K_{cr}$  the spectrum goes continuously to zero, while for  $K \neq K_{cr}$ , like for example for  $K = 0.3$  presented in the figure, its low- $\lambda$  part is cut off at some positive  $\lambda_{min}$ .

- [2] V.A. Kazakov, I.K. Kostov and A.A. Migdal Phys.Lett. **B157** (1985) 295.
- [3] F. David, Simplicial Quantum Gravity and Random Lattices, Les Houches Summer School 1992 Proceedings, hep-th/9303127.
- [4] V.G. Knizhnik, A.M. Polyakov, A.B. Zamolodchikov Mod. Phys. Lett. **A3** (1988) 819.
- [5] F. David, Mod. Phys. Lett **A3** (1988) 509.
- [6] J. Distler and H. Kawai, Nucl. Phys. **B321** (1989) 509.
- [7] M.E. Agishtein, A.A. Migdal, Nucl.Phys. **B385** (1992) 395.
- [8] J. Ambjørn, J. Jurkiewicz Phys.Lett. **B278** (1992) 42.
- [9] P. Bialas, Z. Burda, A. Krzywicki and B. Petersson. Nucl.Phys. **B472** (1996) 293.
- [10] S. Bilke, Z. Burda, A. Krzywicki, B. Petersson, J. Tabaczek, and G. Thorleifsson, Phys.Lett. **B418** (1988) 266.
- [11] H.-C. Ren, Nucl. Phys. **B301** (1988) 661.
- [12] M.A. Bershadsky and A.A. Migdal, Phys. Lett. **B174**, (1986) 393.

- [13] Z. Burda, J. Jurkiewicz and A. Krzywicki, Phys.Rev.**D60** (1999) 105029.
- [14] L. Bogacz, *et al*, Acta Phys. Pol. **B32** (2001) 4121.
- [15] V.A. Kazakov, Phys. Lett. **A119** (1986) 140.
- [16] D.V. Boulatov, V.A. Kazakov, Phys.Lett. **186B** (1987) 379.
- [17] Z. Burda and J. Jurkiewicz, Acta Phys. Polon. **B20** (1989) 949.
- [18] K. Wilson, Phys.Rev. **D10** (1974) 2445.
- [19] K. Wilson, in *New phenomena in subnuclear physics*, ed. A. Zichichi, Plenum Press, N.Y. 1977 (Erice, '75).
- [20] T. Eguchi, P. B. Gilkey and A. J. Hanson, Phys. Rept. **66** (1980) 213.
- [21] M.B. Green, J.H. Schwarz and E. Witten, *String theory*, Cambridge University Press 1987.
- [22] G.H. Golub, C.F. Van Loan, Matrix Computations, John Hopkins University Press 1996.
- [23] S. Catterall, G. Thorleifsson, M. Bowick, V. John, Phys.Lett. **B354** (1995) 58.
- [24] H. Kawai, N. Kawamoto, T. Mogami, Y. Watabiki, Phys. Lett. **B306** (1993) 19.
- [25] H. Kawai, M. Ninomiya, Nucl.Phys. **B336** (1990) 115.
- [26] M.L. Mehta, *Random matrices* New York Acad. Press (1991) ,
- [27] J.J.M. Verbaarschot, I. Zahed, Phys. Rev. Lett.**70** (1993) 3852.
- [28] J.J.M. Verbaarschot, T. Wettig, Ann. Rev. Nucl. Part. Sci. **50** (2000) 343.
- [29] P.H. Damgaard and S.M. Nishigaki, Phys. Rev. **D63** (2001) 045012